Hindawi
Journal of Nanomaterials
Volume 2022, Article ID 3225211, 16 pages
https://doi.org/10.1155/2022/3225211

Research Article

Bioinspired Crosslinked Nanocomposites of Polyvinyl Alcohol-Reinforced Cellulose Nanocrystals Extracted from Rice Straw with Ethanedioic Acid

Kwok-Mern Chin,[1] Sung Ting Sam,[1,2] Hui Lin Ong,[1,3,4] Yee Shian Wong,[5] Wai Kian Tan,[6] and Vilay Vannaladsaysy[7]

[1]*Faculty of Chemical Engineering Technology, Universiti Malaysia Perlis (UniMAP), 02600 Arau, Perlis, Malaysia*
[2]*Centre of Excellence Geopolymer and Green Technology (CEGeoGTech), Universiti Malaysia Perlis, Kompleks Pusat Pengajian Jejawi 2, Taman Muhibbah, 02600 Arau, Perlis, Malaysia*
[3]*Centre of Excellence for Biomass Utilization, Universiti Malaysia Perlis, Lot 17, Kompleks Pusat Pengajian Jejawi 2, 02600 Arau, Perlis, Malaysia*
[4]*Taiwan-Malaysia Innovation Center for Clean Water and Sustainable Energy (WISE Center), Lot 17, Kompleks Pusat Pengajian Jejawi 2, 02600 Arau, Perlis, Malaysia*
[5]*Faculty of Civil Engineering Technology, Universiti Malaysia Perlis (UniMAP), 02600 Arau, Perlis, Malaysia*
[6]*Institute of Liberal Arts and Science, Toyohashi University of Technology, Toyohashi, Aichi 441-8580, Japan*
[7]*Department of Mechanical Engineering, Faculty of Engineering, National University of Laos (NUOL), P.O. Box 3166, Sokpaluang Campus, 01005 Lao-Thai Friendship Rd, Vientiane Capital City, Laos*

Correspondence should be addressed to Sung Ting Sam; stsam@unimap.edu.my
and Vilay Vannaladsaysy; vilay_me@fe-nuol.edu.la

Received 16 March 2022; Accepted 11 June 2022; Published 4 July 2022

Academic Editor: V. Vijayan

In this study, cellulose nanocrystals (CNC) were extracted from rice straw and incorporated into polyvinyl alcohol (PVOH) as reinforcement nanofillers. Multiple nanocomposites with different CNC contents were prepared. Extracted CNC appear as long, well-defined rodlike crystals with a high aspect ratio (41). Nanocomposites with 3 wt% of CNC significantly exhibit improved tensile strength (60.4%) and maximum degradation temperature (287°C). Moreover, they demonstrate a decrease in water vapor permeability rate and in the swelling and solubility indices of PVOH/CNC. Significant improvements were observed when nanocomposites were crosslinked specifically in terms of tensile strength (104.8%) and maximum degradation temperature (364°C). They also demonstrate greatly reduced water vapor permeability rate, swelling, and solubility indices. The optimum CNC amount for both nanocomposites is 3 wt%.

1. Introduction

Plastic is a synthetic polymer that is versatile and durable and has a low production cost; it is also the material of choice for numerous applications worldwide. However, plastics are nondegradable. The significant increase in the use of and dependence on plastics has also increased the waste stream, and this is an issue for the ecosystem and the environment [1–4]. The common nondegradable polymers, such as polyethylene, polypropylene, polyvinyl chloride, and polystyrene, are consumer market dominators that constitute the vast majority of the products that end up in landfills; moreover, they are extremely resistant to degradation [5–10]. In response to this, researchers must design environmentally friendly substitutes (e.g., polymers that are biodegradable when exposed to the environment). One of the most perfect examples of biodegradable synthetic polymers is polyvinyl alcohol (PVOH). PVOH is a conventional water-soluble polymer with a substantial

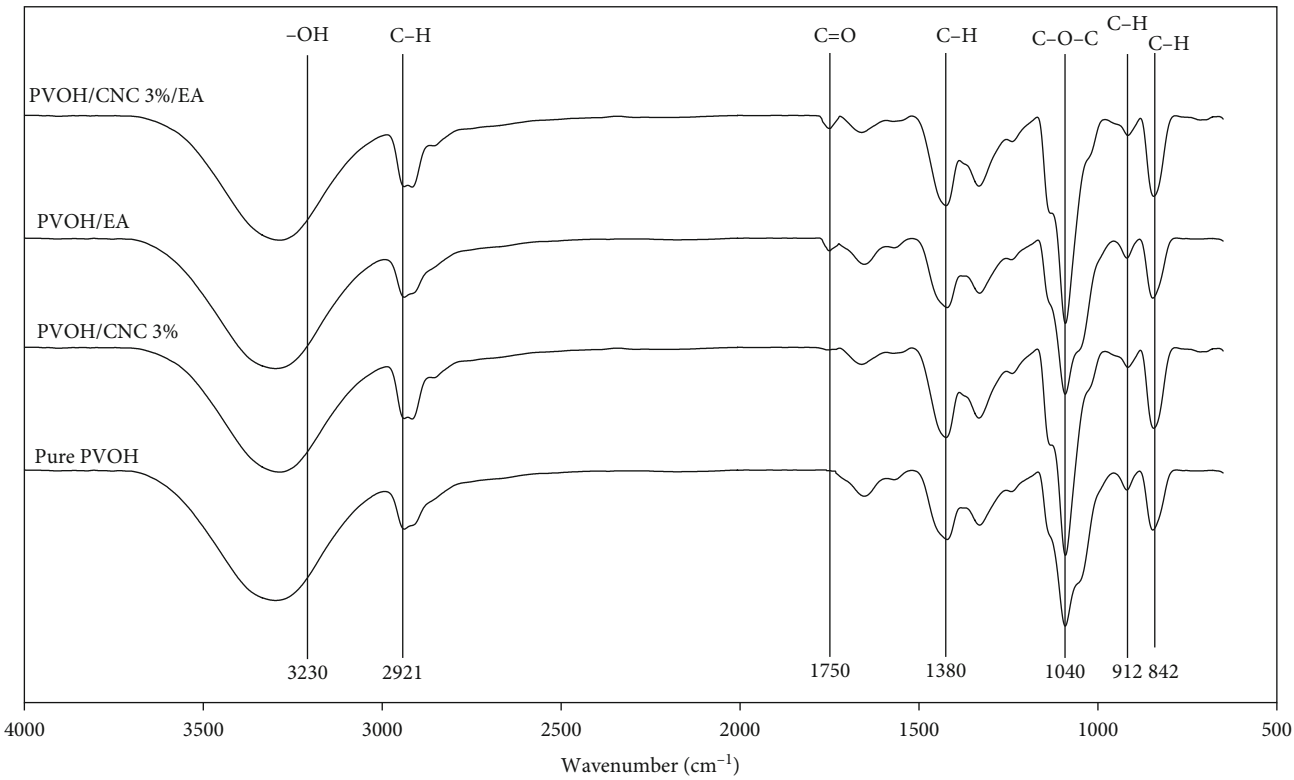

Figure 1: FTIR spectra of pure PVOH, crosslinked PVOH, and crosslinked and non-crosslinked nanocomposites with 3 wt% CNC.

value to the manufacturing industry as it is nontoxic and fully biodegradable and has exceptional biocompatibility [11–13]. PVOH can be adaptively manufactured to suit multiple applications by varying its degree of hydrolysis and its average molecular weight. In addition, PVOH is used in packaging industries owing to its excellent film-forming capability (but only in niche applications due to its water sensitivity).

Researchers are currently focusing on the enhancement and improvement of the properties of neat polymers through the addition of small amounts of inexpensive and environmentally friendly fillers. The conversion of "waste to wealth" is a common interest among the scientific and global communities; thus, agricultural wastes, such as rice straw, sugarcane bagasse, and soy hulls, are the main materials used in the current research. Nanotechnology has warranted exciting opportunities within the realm of material science, especially in the use of nanocellulose derived from renewable sources to improve the properties of polymers as reinforcement filler materials. Nanocellulose exists in multiple forms, namely, cellulose nanocrystals (CNC) and cellulose nanofibers (CNF), depending on the extraction method [14]. CNF are mainly obtained through mechanical fibrillation (a process that requires a huge amount of energy), whereas the production of CNC depends on strong chemical treatment, such as acid hydrolysis [15–18]. Compared with CNF, CNC retain only the crystalline regions of cellulose and are thus preferred [19–23]. However, the inherent hydrophilic nature of CNC with –OH side groups limits their widespread use as reinforcement fillers. The mechanical strength of hydrophobic polymer-reinforced CNC is unfavorable due to the incompatibility between the two counterparts, leading to weak dispersion and serious agglomeration of the CNC [24–26]. To solve these compatibility issues, surface functionalization of nanocellulose, such as TEMPO oxidation, acetylation, acylation, silylation, and polymer grafting, is performed to promote dispersibility of the CNC in hydrophobic polymers by changing the hydrophilic nature of CNC. However, these methods require tedious processing routes and may disrupt the structural integrity of the CNC [27]. Hence, CNC are best utilized in a natural state.

Despite its limitation in widespread applications, neat PVOH can be modified to suit the needs for its end-use application. PVOH crosslinking is one of the best solutions as this method is capable of inducing a tight three-dimensional structured network of molecules that demonstrate hydrophobicity and enhanced properties [28–32]. The hydroxyl groups present in PVOH are the target of reactions, most commonly with chemical compounds, such as dialdehydes, anhydrides, and carboxylic acids [33–38]. Research on crosslinkers such as glutaraldehyde [39–41], epichlorohydrin [42, 43], formaldehyde [44, 45], hexamethoxymethylmelamine [46], and sodium trimetaphosphate [47, 48] indicates that they are not preferable owing to their toxicity. Therefore, the focus of this study is the crosslinking reaction between a natural dicarboxylic acid and ethanedioic acid (EA) on PVOH with different CNC ratios as it is the simplest crosslinking reaction and is environmentally friendly. The tensile properties, degree of crystallinity, and water and thermal stability of non-crosslinked and crosslinked nanocomposites are investigated.

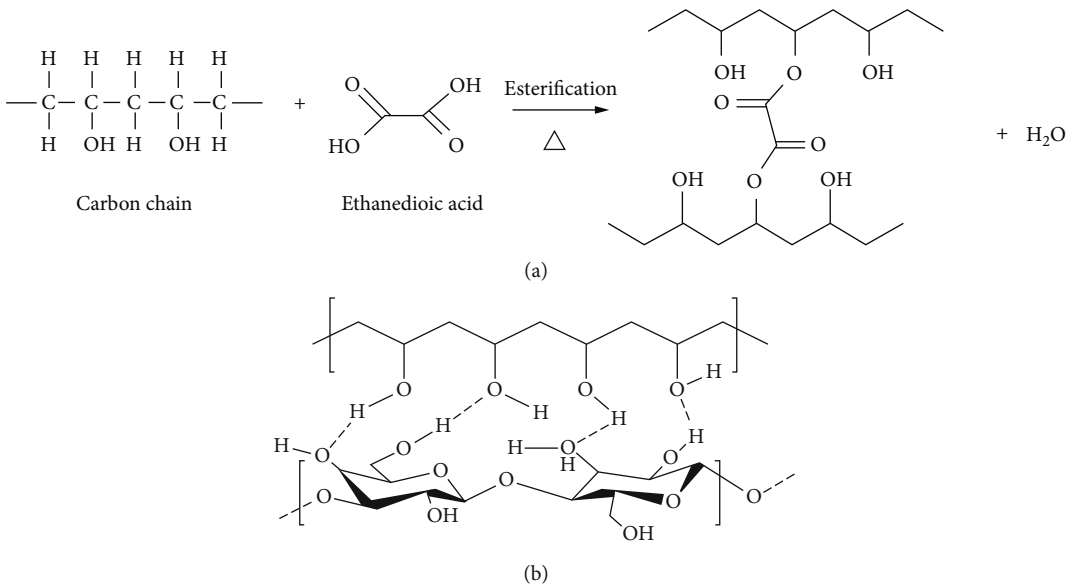

Figure 2: (a) Crosslinking mechanism between PVOH carbon chains with EA. (b) Schematic representation of the interaction between PVOH carbon chains and CNC.

2. Methods

2.1. Materials. Dried rice straw was obtained from a paddy field located in Arau, Perlis, Malaysia (6°25′58.0″N +100°13′56.8″E). PVOH (98% hydrolyzed) with an Mw of 89,000–98,000 was purchased from Sigma-Aldrich (Malaysia). Sodium hydroxide (NaOH), sodium chlorite ($NaClO_2$), and acetic acid glacial (CH_3COOH) was purchased from Merck (Malaysia), Acros Organics (Malaysia), and HmbG (Malaysia), respectively. The sulfuric acid (95%–97%) used for the CNC extraction was purchased from Merck (Malaysia). EA was purchased from Sigma-Aldrich (Malaysia). Deionized water was used consistently throughout the experiment.

2.2. Microcrystalline Cellulose and CNC Extraction. Dried rice straw was washed with water to remove dirt and other impurities before drying in an enclosed environment for 48 h. The rice straw was then converted to a powder form by using a mill grinder prior to separation through a 150 μm mesh screen. Microcrystalline cellulose (MCC) and CNC from rice straw were extracted through alkaline treatment, bleaching, and acid hydrolysis with slight modification to the process described by Chan and coworkers [49]. Next, the separated rice straw powder was treated with a 4% aqueous solution of NaOH (w/w) for a total of 2 h at 80°C under mechanical stirring. Then, the rice straw fiber was washed several times with deionized water until the pH reached 7. Subsequently, the rice straw fiber was bleached with a solution comprising equal parts ($v : v$) acetate buffer (40 g NaOH, 75 mL glacial acetic acid, diluted to 1 L with distilled water) and sodium hypochlorite (1.7 wt% $NaClO_2$). This treatment was performed at 80°C for 2 h under mechanical stirring. The fiber was washed with deionized water until the pH reached 7 again. A total of four cycles of alkaline and bleaching treatment were completed to obtain a milky white MCC pulp. Acid hydrolysis was performed with 64 wt% H_2SO_4 at the optimal temperature of 45°C for 45 min. This process is important to eliminate the amorphous regions of cellulose to achieve the desired highly crystalline CNC. Immediately after 45 min, tenfold of cold deionized water was added to halt the hydrolysis reaction. The suspension was then washed with a copious amount of deionized water and centrifuged at 10,000 rpm. This process was repeated until a CNC suspension with a pH of 6–7 was achieved. Gravimetric method which consist of convection oven drying of CNC at 105°C was adopted to determine the final concentration of CNC in the final suspension after sonication [50].

2.3. Preparation of PVOH/CNC Nanocomposites. PVOH/CNC-film nanocomposites were produced using the solution casting method. PVOH powder was dissolved in water at 90°C with mechanical stirring for 2 h in order to obtain a 2 wt% solution. CNC of known weight percentages (1, 3, 5, and 7 wt%) were added concurrently. For nanocomposite films with EA, 5 wt% of EA was added during the final 30 min to prevent acidolysis. The final solution was poured into a glass mold and oven-dried at 40°C for 24 h. Thermally crosslinked films were obtained via thermal curing of the films with EA in a convection oven at 130°C for 30 min. All the films were stored in a desiccator for 72 h before the measurements were performed.

2.4. Fourier Transform Infrared Spectroscopy. Fourier transform infrared spectroscopy (FTIR) spectra were obtained through a small cut of PVOH/CNC and PVOH/CNC/EA nanocomposite films in the range of 4,000 to 650 cm^{-1} wavenumbers with 32 scans using a PerkinElmer Spectrum 10 spectrophotometer. Beforehand, the samples were washed thoroughly with water and acetone to remove the unreacted excess EA on the surface of the samples. The samples were

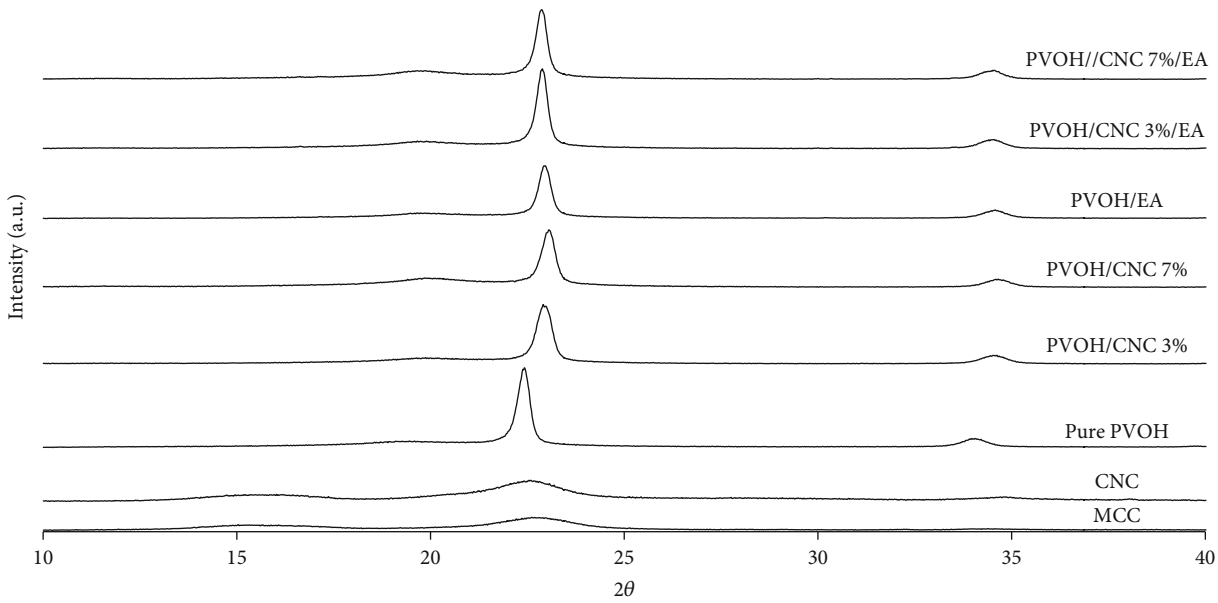

Figure 3: XRD diffractogram of nanocomposites of varying CNC contents with and without the addition of EA.

Table 1: CrI of MCC, CNC, pure PVOH, crosslinked PVOH, and crosslinked and non-crosslinked nanocomposite with 3 wt% and 7 wt% CNC.

Sample	Crystallinity index (CrI)
Pure PVOH	66.1%
PVOH/CNC 3%	70.4%
PVOH/CNC 7%	67.5%
PVOH/EA	65.0%
PVOH/CNC 3%/EA	69.1%
PVOH/CNC 7%/EA	65.5%
MCC	60.8%
CNC	74.3%

then oven-dried to remove moisture before analysis was conducted.

2.5. X-Ray Diffraction. A Bruker D2 Phaser X-ray diffractometer with a monochromatic Cu–Kα radiation source was used to obtain the X-ray diffraction (XRD) patterns of the CNC and the PVOH nanocomposites. The measurement parameters were 0.02° step size in the range of 10° to 40° of a 2θ angle. The crystallinity index (CrI) was determined by calculating the peak area from the diffraction peaks using the Segal method. The formula of the calculation is as follows:

$$\text{Crystallinity index (CrI)} = \frac{(I_{002} - I_{AM})}{I_{002}} \times 100, \quad (1)$$

where CrI denotes the degree of crystallinity (%), I_{002} is the maximum intensity of 0 0 2 lattice diffraction, and I_{AM} is the diffraction intensity at $2\theta = 18°$.

2.6. Tensile Properties. The tensile properties of the nanocomposite films were examined on a universal testing machine (Instron 5567) in accordance with the ASTM D-882 standard procedure. A total of five 100 × 10 mm rectangular samples were cut precisely from the nanocomposite films, and the test was conducted at a crosshead speed of 20 mm/min. The tensile strength, elongation at break, and Young's modulus were obtained.

2.7. Field Emission Scanning Electron Microscopy. The surface morphology of the tensile-fractured surfaces of the nanocomposite films was observed using a field emission scanning electron microscope (FESEM, Carl Zeiss Leo Supra 50 VP Field Emission). A small cut of the fractured surface from each of the nanocomposites was adhered onto the specimen stage with carbon tape. All the samples were sputter-coated with platinum before they were examined at an accelerated voltage of 5 kV under a high-vacuum condition.

2.8. Transmission Electron Microscopy. To determine the morphology of the CNC, 10 μL of 0.005 wt% CNC suspension was placed on a transmission electron microscopy (TEM) grid for 2 min. Excess liquid was removed with filter paper, followed by negative staining with uranyl acetate solution for another 2 min. Excess uranyl acetate solution was blotted with filter paper before letting the CNC dry at an ambient temperature. The CNC were observed under a transmission electron microscope (LIBRA 120) at 100 keV. The average length and diameter of the CNC were determined from 50 representative CNC using the ImageJ and Origin software. Gaussian distribution curves were obtained using the Origin software.

2.9. Thermogravimetric Analysis. Thermogravimetric analysis (TGA) and derivative thermogravimetry (DTG) curves were obtained through the thermal behavior analysis of the

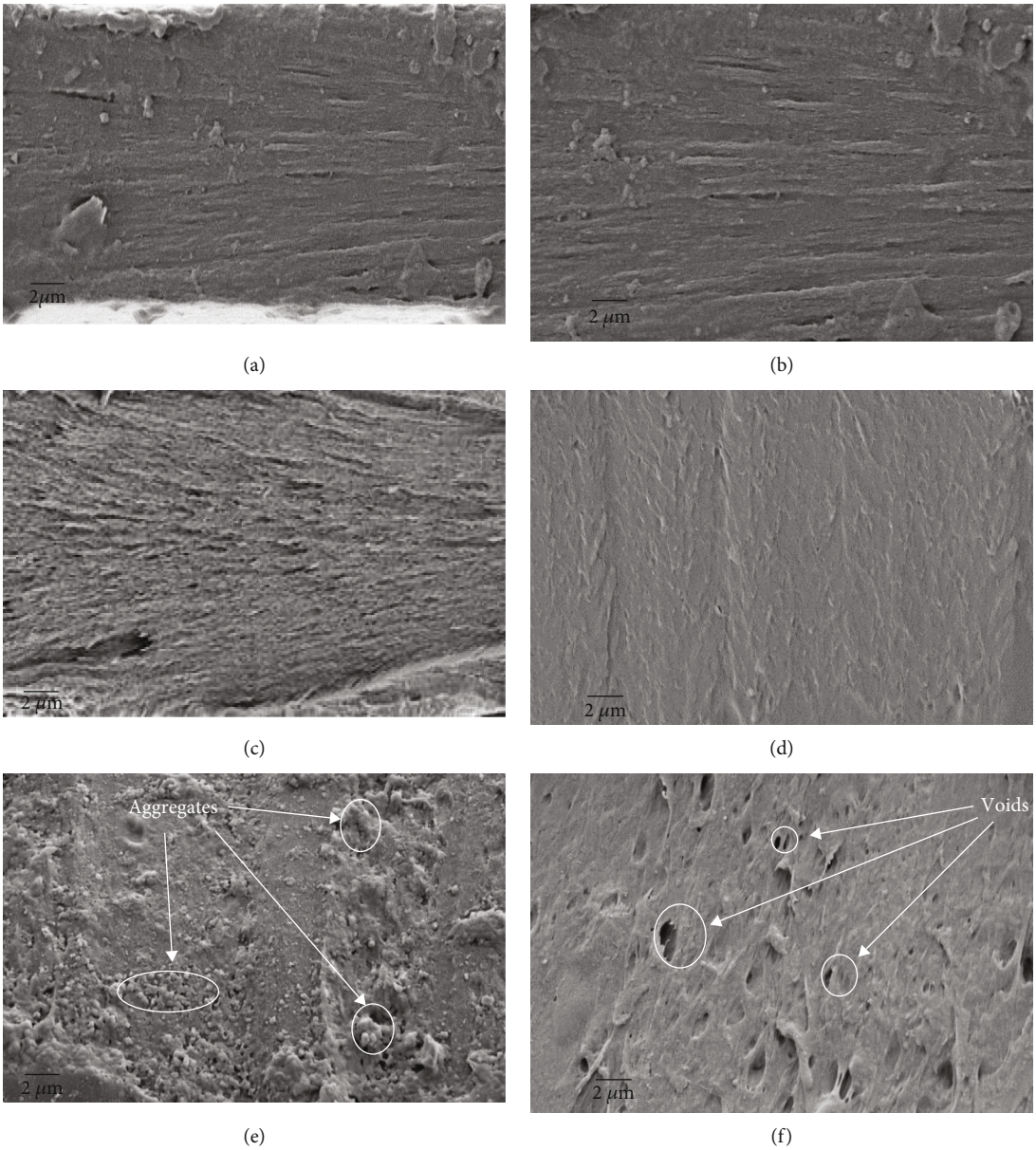

Figure 4: FESEM micrographs of (a) pure PVOH, (b) crosslinked PVOH, (c) 3 wt% PVOH/CNC, (d) crosslinked 3 wt% PVOH/CNC, (e) 7 wt% PVOH/CNC, and (f) crosslinked 7 wt% PVOH/CNC. Magnification: ×3,000.

nanocomposites using a thermogravimetric analyzer (TGA Q50 V20.13 Build 39). A nanocomposite film (estimated weight: 5 mg) was cut and placed on the heating pan before heating from room temperature to 650°C at a rate of 10°C/min. Nitrogen gas purging was performed before the start of the measurement. The temperature values obtained when the weight loss of the sample reached 10% and 30% of the original weight are denoted as $T_{10\%}$ and $T_{30\%}$. T_{MAX} is the temperature at maximum weight loss of the sample.

2.10. Moisture Vapor Permeation Rate. The moisture vapor permeation (MVP) rate was determined in accordance with the wet-cup method (ASTM E96). Glass bottles with a mouth opening of 1 cm^2 were filled with deionized water and sealed with adhesive to prevent the escape of water vapor. The film samples were placed on top of these bottles and in a humidity chamber that was set to maintain an ambient temperature of 25°C with a relative humidity of 40%. The weight of the bottle was determined every 24 h for 7 days. The MVP was calculated using

$$\mathrm{MVP} = \frac{\mathrm{W_{before}}}{\mathrm{A} \times \mathrm{t}}. \quad (2)$$

W_{before} is the initial weight of the bottle filled with water and nanocomposite film. A is the mouth area of the bottle. t is the time (hours).

2.11. Swelling and Solubility Indices. Nanocomposite films (5 × 5 cm) were prepared and immersed in 100 mL deionized water for 24 h at room temperature. After 24 h, the nanocomposite films were removed and dried using filter paper

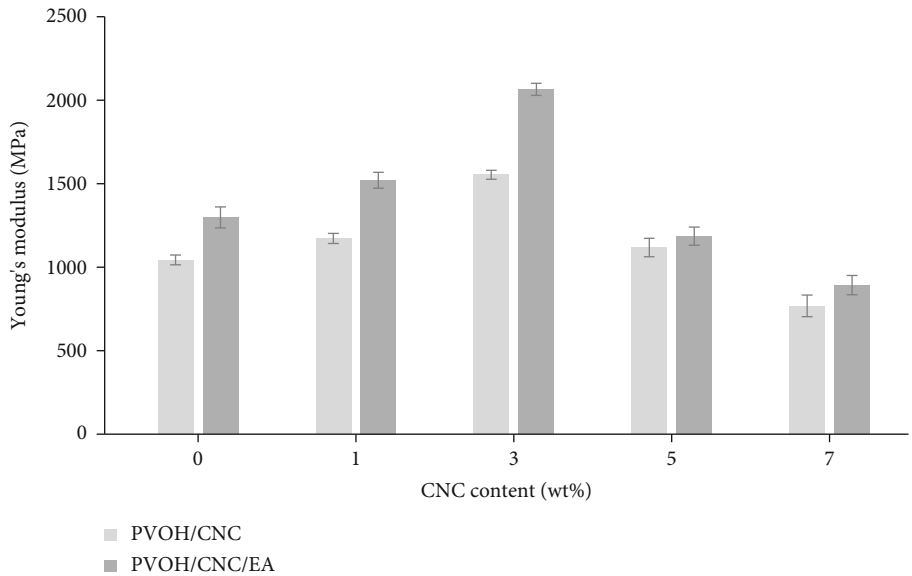

Figure 5: Young's modulus of the nanocomposites with varying CNC contents with and without the addition of EA.

before the weight gain and swelling were measured. The swelling index (SwI) was calculated using Equation (3). Due to the difficulty of the dissolution of fully hydrolyzed PVOH in water at room temperature, the solubility index (SoI) was determined through film immersion in heated deionized water (90°C) for 15 min. SoI was calculated using Equation (4).

$$\mathrm{SwI} = \frac{W_{\mathrm{gain}} - W_{\mathrm{initial}}}{W_{\mathrm{initial}}}, \quad (3)$$

$$\mathrm{SoI} = \frac{W_{\mathrm{initial}} - W_{\mathrm{remain}}}{W_{\mathrm{initial}}}. \quad (4)$$

W_{initial} is the initial weight of the sample. W_{gain} is the weight gain of the sample. W_{remain} is the remaining weight of the sample.

3. Results and Discussion

3.1. FTIR. Figure 1 presents the FTIR spectra of pure PVOH, crosslinked PVOH, and crosslinked and non-crosslinked nanocomposites with 3 wt% CNC. There are minor differences in the spectrum curves between the parallel compositions of nanocomposites. The broad peak at 3,230 cm^{-1} of all the nanocomposites indicates the availability of the –OH groups in the intermolecular and intramolecular hydrogen bonding between PVOH and CNC [51]. The peak at 2,921 cm^{-1} for all the nanocomposites indicates the vibration of the aliphatic C–H alkyl groups. The bands appearing at wavenumbers of 912 and 842 cm^{-1} show the presence of the stretching vibrations of the C–H bond in PVOH [52]. For the crosslinked nanocomposites, the appearance of a small peak at 1,750 cm^{-1} proves the success of the crosslinking reaction due to the formation of ester C=O bonds [53]. The peak at the wavenumber of 1,680 cm^{-1} for all nanocomposites is due to the presence of adsorbed water, whereas the peak at 1,380 cm^{-1} indicates the presence of the C–H vibration band. The peak intensity increased for the nanocomposites with CNC at 1,040 cm^{-1} (but it did not for pure PVOH) due to the C–O–C vibration from the pyranose ring present in the cellulose [32].

3.2. Interactions between Polyvinyl Alcohol, Cellulose Nanocrystals, and Ethanedioic Acid. As presented in Figure 2(a), the crosslinking mechanism is attributed to the esterification reaction between PVOH and EA. Intermolecular diester bonds are formed as a result of the linkage between the carboxyl groups of EA with the hydroxyl groups of PVOH in high-temperature environments (as was proven in Section 3.1). Either one or both carboxylic acid end groups of EA will react with the hydroxyl end group of PVOH, resulting in the formation of strong crosslink bridges that improve the SwI, SoI, and tensile properties of the nanocomposites. Conversely, Figure 2(b) presents the interaction between the hydroxyl groups of PVOH and CNC through the formation of hydrogen bonds.

3.3. X-Ray Diffraction. Figure 3 presents the XRD diffraction patterns of MCC, CNC, pure PVOH, crosslinked PVOH, and crosslinked and non-crosslinked nanocomposites (3 and 7 wt%). The well-defined characteristic peaks of the cellulose type I lattice structures, occurring around 16.1° and 22.4°, are observed for CNC [54]. The unaltered diffraction peaks of the CNC in comparison with MCC confirm that the acid hydrolysis treatment employed to extract CNC through the removal of unwanted amorphous regions did not affect the crystalline nature of the cellulose. The narrower and sharper peak demonstrated by CNC at 22.4° indicates that it exhibits a better crystal lattice structure and a higher cellulose index than MCC [55, 56]. This translates to a greater reinforcing ability on the tensile properties of PVOH (discussed in Section 3.6). As presented in Table 1, the CrI of CNC increased to 74% due to the release of

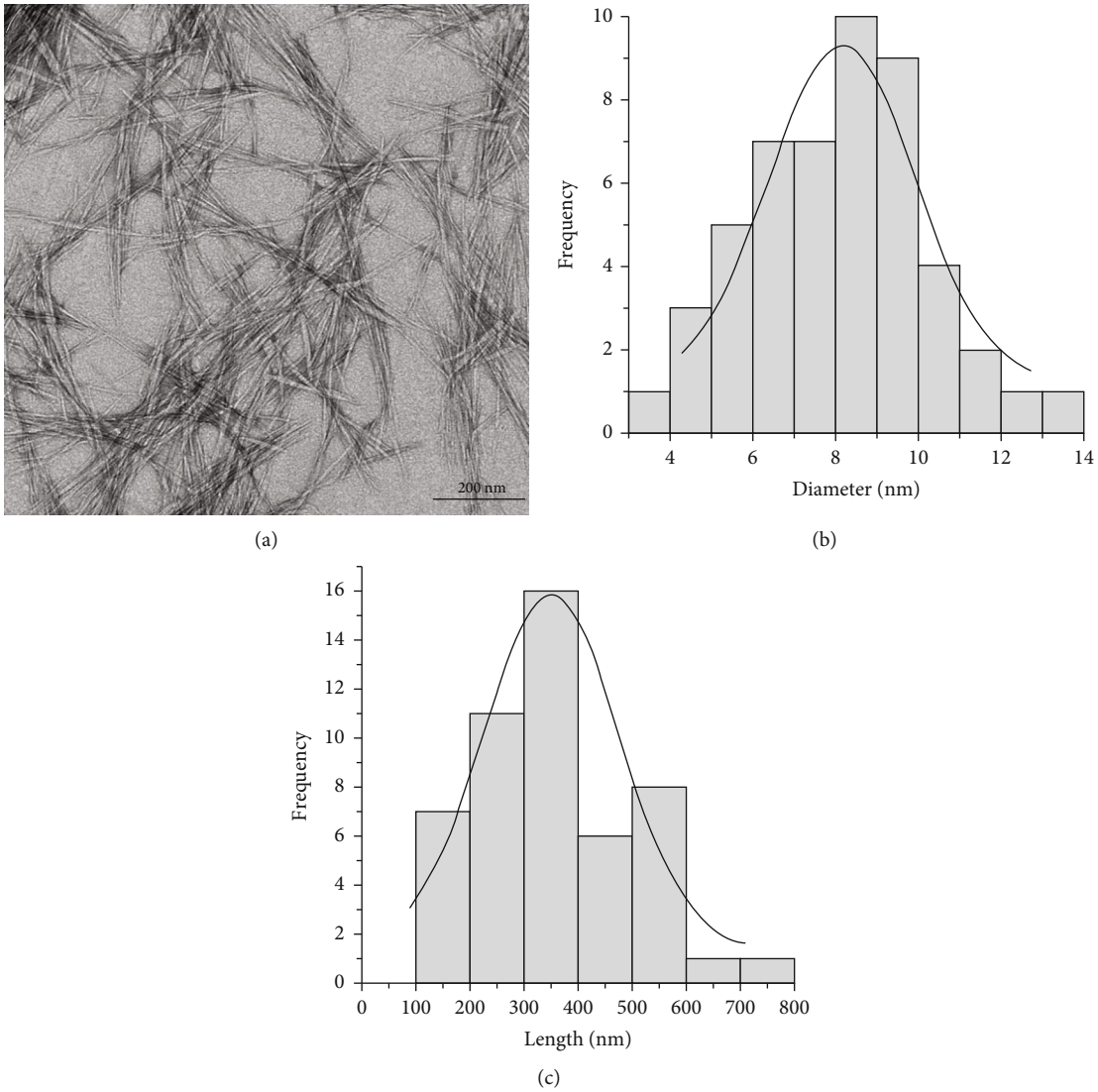

Figure 6: TEM image of (a) CNC extracted from rice straw with their (b) diameter and (c) length distributions. Magnification: ×25,000.

individual crystallites from the hydrolytic cleavage of the glycosidic bonds in the amorphous regions. For both the non-crosslinked and crosslinked nanocomposites, the CrI improved with the addition of CNC due to the increase in the amount of crystalline material in the system [57]. At a higher filler content of CNC (7 wt%), the CrI decreased. This is mostly due to the effect that the steric hindrance of CNC, which is the retardation of chemical reactions that disrupts the formation of intermolecular bonds between molecules, has on the organized structure of the carbon–carbon polymer chains in PVOH. A similar occurrence was reported by Hoseini et al. [58] when the CrI dropped during high carbon nanotube loading in a polyamide-6 polymer. The addition of EA as the crosslinker decreased the CrI of the nanocomposites. This occurred because after crosslinking, the interactions between the PVOH chains limited the mobility of the molecular chain motion, hampering the crystallization process and negatively affecting the crystallinity of the crosslinked films. A similar decrease in crystallinity findings was observed by Nataraj et al. [59] when chitosan films were crosslinked with citric acid. Wu et al. [60] also reported a decrease in peak intensity (indicating a drop in the percentage of crystallinity) after crosslinking starch films with citric acid.

3.4. Tensile Fracture Surface. Figures 4(a)–4(f) present the FESEM micrographs of the tensile-fractured surfaces of non-crosslinked and crosslinked nanocomposites exhibiting different morphologies. From Figures 4(a) and 4(b), it can be observed that the crosslinking of pure PVOH resulted in a much smoother fracture surface when compared with pure PVOH. Similar findings were reported by Jain et al. [61] on crosslinked PVOH with hydrochloric acid. Figure 4(c) presents a rougher, bristly cross-sectional fracture due to the existence of strong interactions between the CNC and PVOH matrix. These findings indicate that the non-crosslinked 3% nanocomposite suffered from a brittle fracture. This is also supported by the results presented in Figure 5, in which the incorporation of CNC increased Young's modulus, thereby increasing the brittleness of the

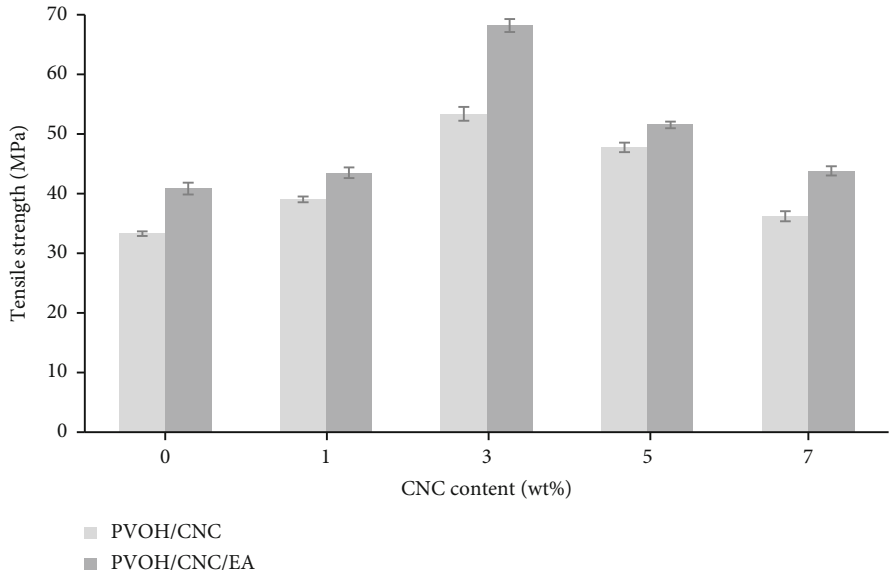

Figure 7: Tensile strength of the nanocomposites with varying CNC contents with and without the addition of EA.

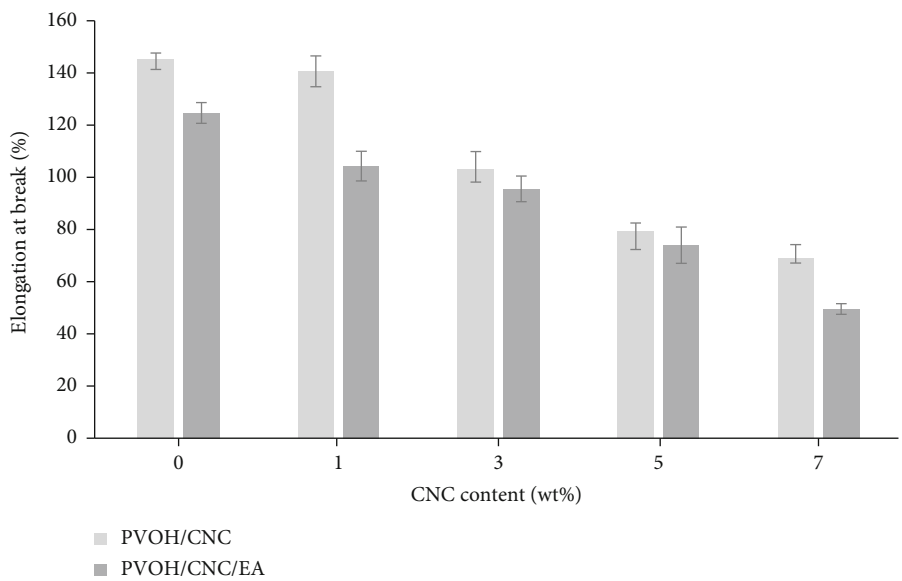

Figure 8: Elongation at break of the nanocomposites with varying CNC contents with and without the addition of EA.

nanocomposite. As can be seen from Figure 4(d), the crosslinked 3% nanocomposite exhibited a smoother, wavelike fracture surface structure, suggesting a relative homogeneous dispersion of CNC within the nanocomposite. Similar findings were also obtained in PVOH/functionalized CNC composite films by Chen et al. [62]. There are also no observable internal cracks or phase separations attributed to the greater tensile strength of crosslinked nanocomposites when compared with non-crosslinked nanocomposites [62]. In Figures 4(e) and 4(f), the voids, aggregates, and coarser surfaces shown throughout the fracture surfaces led to a weaker transfer of strength. This directly translated to a decrease in tensile strength and Young's modulus.

3.5. Morphology. As can be seen from Figure 6(a), the CNC extracted from rice straw appeared as long, well-defined rod-like crystals. The Gaussian distribution for the CNC diameter presented in Figure 6(b) confirmed that it was in the range of 3–14 nm. The standard deviation, reduced chi-squared, and R-squared values obtained were 2.1 nm, 1.3, and 0.88, respectively. As can be seen from Figure 6(c), the length of the CNC obtained was in the range of 100–800 nm. The standard deviation, reduced chi-squared, and R-squared values obtained were 139.0 nm, 9.74, and 0.68, respectively. The average length was 331.97 nm, and the average diameter was 8.11 nm. The aspect ratio of the CNC, calculated from the ratio of the length over the

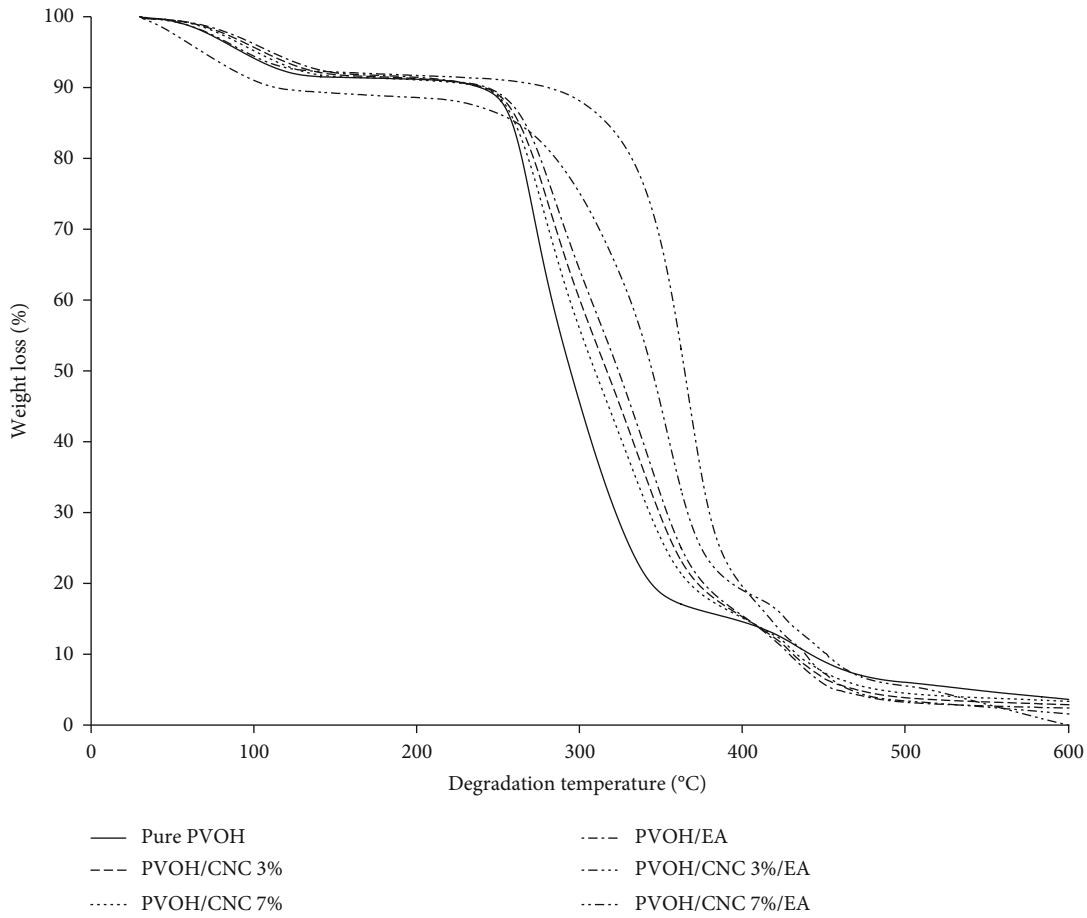

Figure 9: Thermogram of the nanocomposites with varying CNC contents with and without the addition of EA.

Table 2: TGA data from the thermal decomposition of nanocomposites with varying CNC contents with and without the addition of EA.

Sample	$T_{10\%}$ (°C)	$T_{30\%}$ (°C)	T_{MAX} (°C)
Pure PVOH	239	273	275
PVOH/CNC 3%	241	285	287
PVOH/CNC 7%	240	281	282
PVOH/EA	243	291	342
PVOH/CNC 3%/EA	280	348	364
PVOH/CNC 7%/EA	213	312	356

diameter, was 41. This value was higher than the aspect ratio of the rice straw CNC extracted by Lu and Hsieh [63]. This result demonstrated that the preliminary cyclic treatment performed on the CNC, prior to extraction, was effective. Moreover, the aspect ratio reported in this study was higher than that of the CNC extracted from other reported cellulosic sources, such as commercial MCC (16.8), corncob (37), switchgrass (38), cotton (13), and onion skin (10.1) [64–67].

3.6. Tensile Properties. Figure 7 presents the comparison of the tensile strengths of the crosslinked and non-crosslinked nanocomposites with varying CNC contents. The tensile strength of non-crosslinked nanocomposites improved (increasing in value to 60.4%) as the CNC content increased up until 3 wt%. The crosslinked nanocomposites also demonstrated an upward trend, but the increase was much more pronounced (up to 104.8%) due to additional factors, such as the improved transfer of strength from the crosslinking network to the nanocomposite. The excellent compatibility of PVOH with CNC facilitated the homogeneous distribution of the CNC throughout the PVOH, as is shown in Figure 4(c). This, coupled with the success of hydrogen intermolecular and intramolecular bond formation, led to the positive enhancement in tensile strength. The nature of CNC, which is widely known to be strong and possess large interfacial surface area, also contributed to such an enhancement [68]. In CNC above 3 wt% for both the crosslinked and non-crosslinked nanocomposites, factors such as reaching the filler-saturation point and agglomeration start to exert detrimental effects on the tensile strength of the nanocomposites [69]. In the case of the crosslinked nanocomposites, the improvement in tensile strength is attributed to the formation of the crosslink bridges through the intermolecular ester bonding between the PVOH chains (as is illustrated in Figure 2(b)). This interaction within the matrix contributed to the development of a more compact structure than the non-crosslinked nanocomposites. The drop in strength

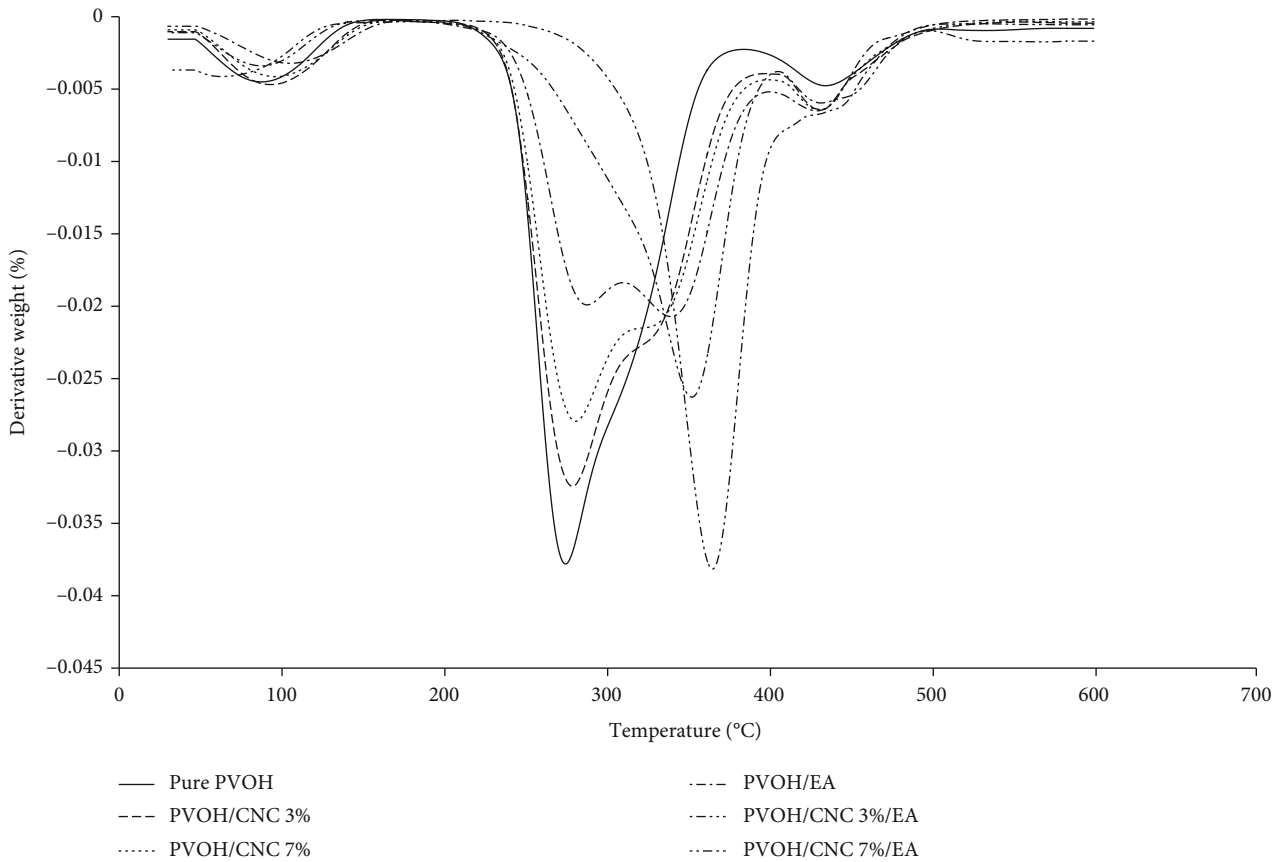

Figure 10: Differential thermogravimetry (dTG) curve of the nanocomposites with varying CNC contents with and without the addition of EA.

beyond 3 wt% may be due to the reduced availability of the hydroxyl groups as they were already used to form the crosslinks. A reduced number of hydroxyl groups prevents excess CNC from forming hydrogen bonds with PVOH, leading to unreacted CNC. This unreacted CNC agglomerates, forming random localized weak points on the nanocomposite.

Figure 8 presents the comparison of elongation at break values between crosslinked and non-crosslinked nanocomposites with varying CNC contents. In all cases, the increase in the amount of CNC slightly reduced the elongation of break in nanocomposites due to the addition of CNC with known stiff and rigid structures as reinforcement filler materials [68]. Consequently, the ductility of the nanocomposites was reduced (due to the diminishing content of PVOH) when the CNC content increased. A similar trend was observed in crosslinked nanocomposites in which the elongation of break was found to be much lower than that of non-crosslinked nanocomposites. Such a reduction in elasticity after crosslinking indicates that the nanocomposites lost their ductile nature as their polymer chain mobility was reduced by the formation of crosslinked networks. Jose reported similar findings when citric acid was used as the crosslinker for PVA/starch/graphene nanocomposites [70]. The elongation at break values was also found to decrease when glutaraldehyde was used a crosslinking agent in polyvinyl alcohol/chitosan composites [71]. There is even a phenomenon demonstrating that crosslinkers exert a plasticizing effect, but this is at the expense of tensile strength. Wu et al. [60] demonstrated that when a higher citric acid content was used for crosslinking, the elongation at break was favored, but it significantly reduced the tensile strength. The unreacted excess citric acid content acted as the plasticizer, reducing the interactions between the PVOH carbon chains. Therefore, the incorporation of crosslinking agents in optimum amounts can improve the properties of the nanocomposites. However, any excess crosslinking agent will act as a plasticizer and cause a negative impact.

The significant increase in Young's modulus for both crosslinked and non-crosslinked nanocomposites up until 3 wt% is presented in Figure 5. With 1 wt% CNC content in non-crosslinked and crosslinked nanocomposites, the increase in Young's modulus was 12% and 17%, respectively. With 3 wt% CNC in non-crosslinked and crosslinked nanocomposites, the highest increase in Young's modulus was approximately 49% and 59%, respectively. The addition of stiff CNC to the polymer matrix led to the formation of rigid CNC networks that translated to the stiffness and improved strength of the nanocomposites. The 3 wt% CNC non-crosslinked nanocomposites exhibited a greater increase in Young's modulus than PLLA-grafted CNC with a similar CNC weight percentage [72]. Young's modulus also significantly increased after crosslinking. Ben Shalom et al. [73] reported that crosslinking of PVOH/CNC with 1,2,3,4-butanetetracarboxylic acid further improved the stiffness and strength of the composites. These findings are in agreement with the results presented in Figure 5.

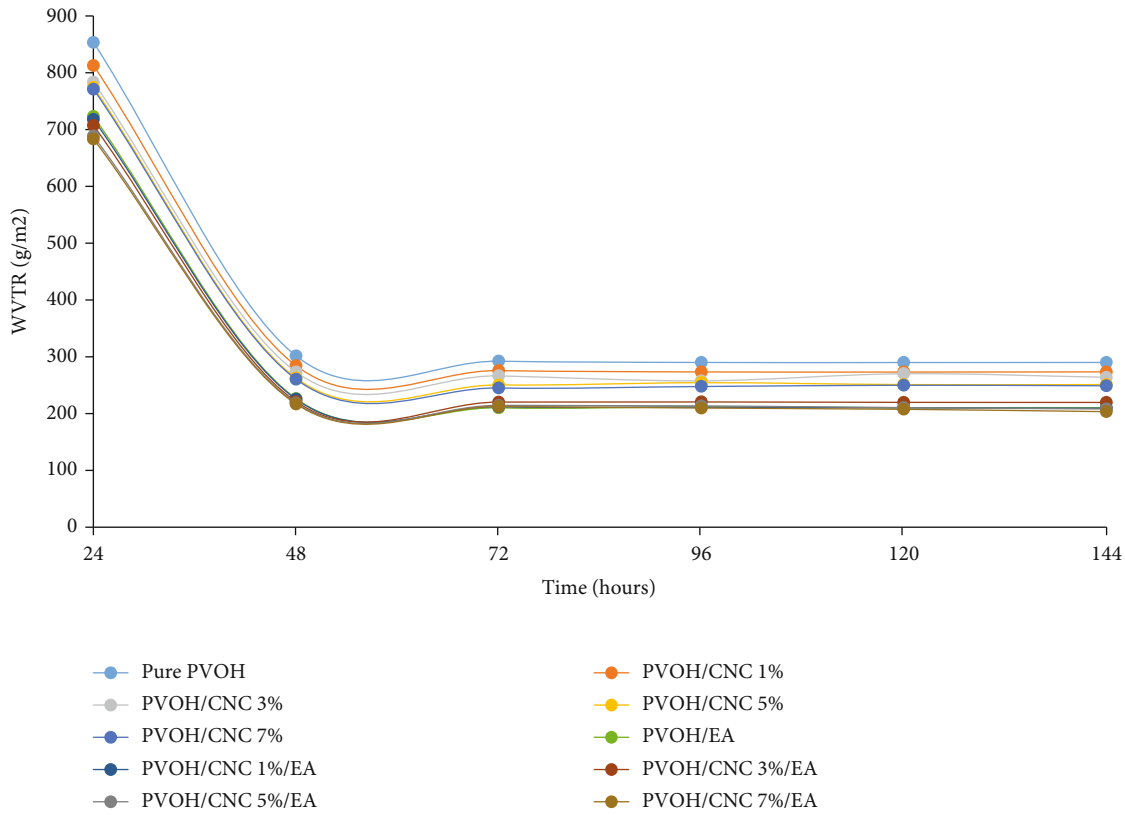

Figure 11: The MVP of nanocomposites with varying CNC contents with and without the addition of EA.

3.7. Thermogravimetric Analysis. TGA was conducted to analyze the thermal behavior of crosslinked and non-crosslinked nanocomposites of varying CNC contents. The three important regions of weight loss are disclosed in the thermogravimetric curve presented in Figure 9. The initial weight loss occurred at approximately 40°C–100°C and is observed for all nanocomposites. This event is attributed to the loss of water through evaporation, mostly of free bound water molecules that are loosely attached to the surface of the nanocomposites [44]. The next weight loss event occurred at around 210°C–400°C and is attributed to the degradation of the nanocomposites. The nanocomposites lost approximately 70% of their total weight, and this region is the most important for indicating their thermal stability. Weight loss is mainly attributed to the degradation of volatile products such as intrinsic water content and unsaturated compounds.

The last weight loss event occurred at greater than 400°C (at approximately 440°C) and is attributed to the degradation of polyene, hydrocarbons, and chain scission of the nanocomposites [74]. As presented in Table 2, crosslinked nanocomposites were found to exhibit greater $T_{10\%}$, $T_{30\%}$, and T_{MAX} values. After the occurrence of crosslinking, the $T_{10\%}$, $T_{30\%}$, and T_{MAX} values of pure PVOH increased from 239°C, 273°C, and 275°C to 243°C, 291°C, and 342°C, respectively. A similar increase was observed for the $T_{10\%}$, $T_{30\%}$, and T_{MAX} values of crosslinked PVOH with the addition of CNC, from 241°C, 285°C, and 287°C to 280°C, 348°C, and 364°C, respectively. The increase in the thermal decomposition temperature indicated the occurrence of crosslinking. These results are in agreement with the findings of Stelescu et al. [75] in which the occurrence of crosslinking of ethylene propylene diene monomers with butyl rubber composites was proven by the resulting improvement in the $T_{10\%}$, $T_{30\%}$, and T_{MAX} values. This improvement is highly beneficial as the crosslinked nanocomposites are more thermally stable and more resistant to thermal degradation.

Figure 10 presents the derivative weight loss curve of the nanocomposites. Crosslinked PVOH had four degradation steps, whereas pure PVOH and the other nanocomposites had only three degradation steps. Sonker et al. [76] reported similar findings on crosslinked PVOH with suberic acid and terephthalic acid. For the crosslinked nanocomposites with 3 and 7 wt% of CNC, the addition of CNC caused the second and third steps to coalesce, forming only one strong derivative weight peak. Song et al. [77] presented similar findings on the thermal degradation steps for the Fenton free radical crosslinking of PVOH with the addition of CNC. It is also evident in Figure 10 that the addition of CNC increased the maximum degradation temperature of the nanocomposite with 3 wt% CNC but reduced it when 7 wt% CNC was added. At higher filler content, factors such as CNC agglomeration dominated, and the thermal stability of the nanocomposites was reduced. A comparable occurrence on the thermal behavior of PVOH/CNC extracted from commercial cellulose at higher filler loading was also demonstrated in the report by Song et al. [77]. The degradation peak from

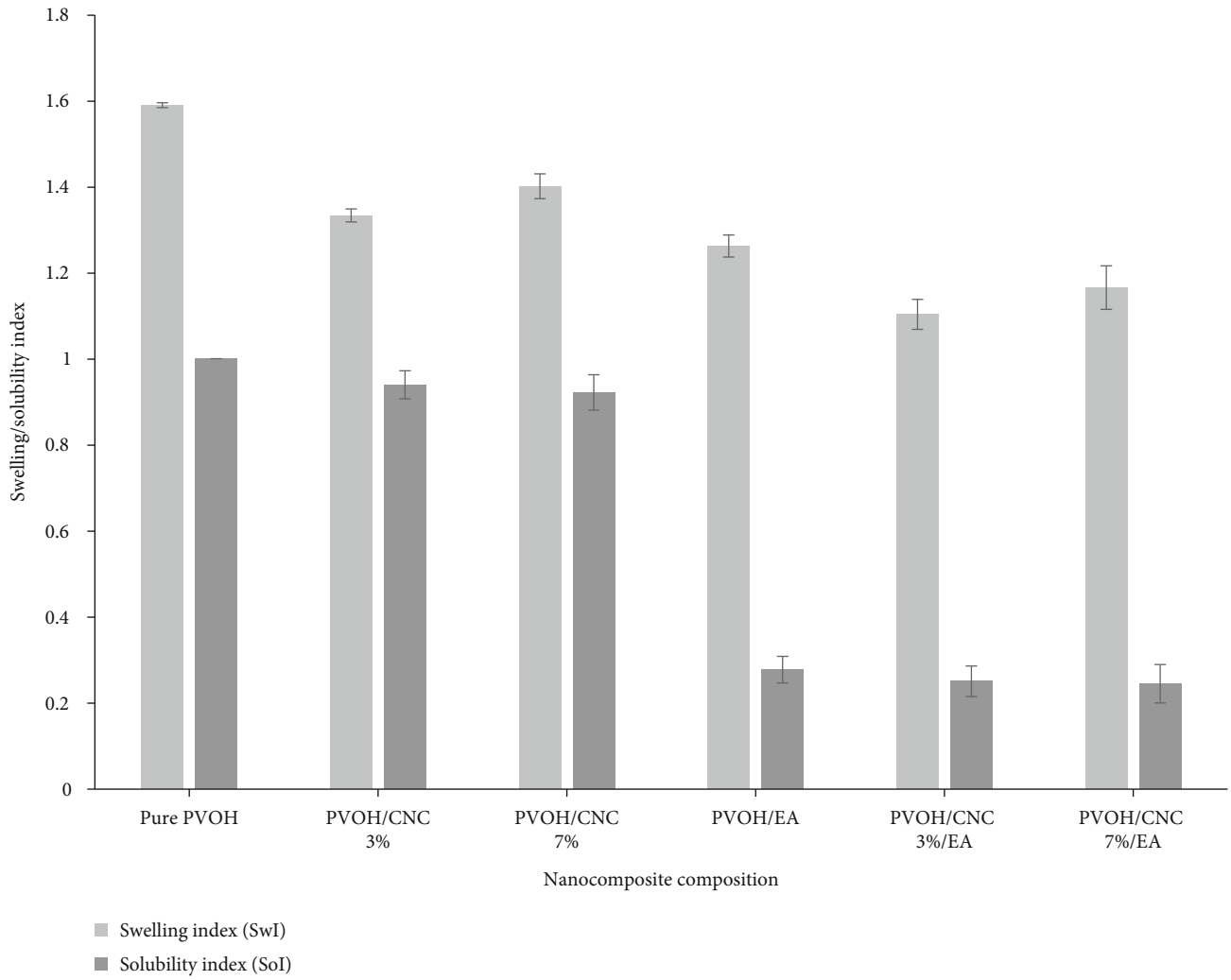

Figure 12: SoI and SwI of the nanocomposites with varying CNC contents with and without the addition of EA.

the DTG curve indicates an increased thermal stability of the nanocomposites with 3 and 7 wt% CNC when compared with pure PVOH. As presented in Table 2, the T_{MAX} value significantly increased after crosslinking, most prominently for the nanocomposites with 3 wt% (from 287°C to 364°C). The obvious shift of the peak of the crosslinked nanocomposites to the right indicated that there is a great improvement in thermal stability.

3.8. Water Vapor Permeation Rate. The MVPs of crosslinked and non-crosslinked nanocomposites with varying CNC contents are presented in Figure 11. Moisture vapor transmission through films (especially hydrophilic films) independently varies with its degree of hydrophilicity. Moisture tends to interact with the polymeric matrix of the film, increasing its moisture permeability. Non-crosslinked nanocomposites are more inclined to have a higher MVP value compared with crosslinked nanocomposites owing to their higher hydrophilic behavior. During the initial exposure of nanocomposite films to moisture, swelling slowly occurs, causing distortions in the polymer chain conformation within the films [78, 79]. At 48 h, the MVP value starts to taper and remains at a steady state. Water, acting as a plasticizer, loosens the polymer chains, which leads to an increase in the MVP [80]. Pure PVOH most clearly demonstrates this effect. The addition of CNC substantially reduced the MVP value for all the nanocomposites. At higher CNC concentrations, most of the water molecules are blocked from passing through the polymer matrix, as the increase in CNC disrupts the water molecule pathways. CNC significantly reduces the diffusibility of moisture vapor owing to its size and swelling constraints, as well as its strong network formation in nanocomposite films. Nair et al. [81] obtained similar findings on the reduction in the MVP of nanocellulose films. The reduction in the MVP is more pronounced with crosslinked nanocomposites with increased CNC content. This is due to the synergistic effect from the crosslinked bridges with CNC, thereby favoring their application as thin packaging films for moisture-sensitive materials, such as food and beverage products [82].

3.9. Solubility and Swelling Index. The SoI and SwI are presented in Figure 12. The results indicate that the SoI of the crosslinked nanocomposites significantly decreased when

compared with that of the non-crosslinked nanocomposites, from an estimated index of 1 to 0.25. This result proves that the proposed crosslinking reaction with EA (as was discussed in Section 3.2) was successful as it increased the hydrophobicity of the nanocomposites to water. However, the addition of CNC only minimally affected the SoI index. This is likely due to CNC's similar hydrophilic nature to the polymer matrix. The SwI was at its lowest in the 3 wt% of PVOH/CNC nanocomposite when compared with pure PVOH and the nanocomposite with 7 wt% of CNC. A similar trend was observed for the crosslinked nanocomposites. PVOH is a hydrophilic material that tends to easily attract water molecules owing to its free hydroxyl groups. The difference in the swelling behavior is attributed to its crystallinity, where the non-crosslinked nanocomposite films with higher CrI values augmented the difficulty of the water to penetrate the PVOH network [83]. The formation of dense, three-dimensional network structures as a result of crosslinking additionally reduced the intermolecular spaces. This favorably affected the SwI value (even at a lower CrI value) for the non-crosslinked nanocomposites [84, 85]. According to Alessandra Bersanetti et al. [84], the reduction in the SwI after crosslinking was due to the diminished availability of excess hydroxyl groups to form hydrogen bonds with water molecules. In the case of PVOH with 7 wt% CNC, for both crosslinked and non-crosslinked nanocomposites, agglomerated and unreacted CNC imparted voids and imperfections throughout the film, which are presented in Figures 4(e) and 4(f), respectively. These findings consequently resulted in an increase in the SwI.

4. Conclusion

This study successfully extracted cellulose nanocrystal (CNC) from rice straw and used it as a reinforcement filler on polyvinyl alcohol. The utilization of EA as a crosslinker proved successful and produced very favorable results. A distinctive improvement in the tensile strength and Young's modulus of non-crosslinked nanocomposites and an even greater improvement in crosslinked nanocomposites were observed. The XRD data indicated that there was an increase in the degree of crystallinity of the nanocomposites when CNC was added. After crosslinking, the nanocomposites exhibited a decrease in the degree of crystallinity. The extracted CNC had a high aspect ratio of 41 and appeared as long, well-defined rodlike crystals. The maximum degradation temperature of the nanocomposites increased at the optimum content of 3 wt% CNC. An additional increase was observed after crosslinking. Crosslinking reduced the values of MVP, solubility index, and swelling index, favoring its application in thin-film packaging for moisture-sensitive materials. Although the addition of CNC is promising and this study revealed its benefits by improving on certain niche properties of PVOH, it does not favor widespread use. Crosslinking of the nanocomposite to drastically reduce its hydrophilicity and significantly improve its tensile and thermal properties must be performed before it can be widely used. In conclusion, the optimum CNC content was 3 wt% for both crosslinked and non-crosslinked nanocomposites.

Data Availability

The experimental data used to support the findings discussed in this study are included within the article.

Conflicts of Interest

The authors declare no conflict of interest.

Acknowledgments

The authors are thankful to Universiti Malaysia Perlis for providing the facilities necessary to perform this research. This research was performed as a part of the employment of Universiti Malaysia Perlis.

References

[1] C. A. Bernardo, C. L. Simões, and L. M. C. Pinto, "Environmental and economic life cycle analysis of plastic waste management options. A review," in *AIP Conference Proceedings*, vol. 1779, Graz, Austria, 2016.

[2] L. C. M. Lebreton, J. Van Der Zwet, J. W. Damsteeg, B. Slat, A. Andrady, and J. Reisser, "River plastic emissions to the world's oceans," *Nature Communications*, vol. 8, no. 1, pp. 1–10, 2017.

[3] J. Vince and B. D. Hardesty, "Plastic pollution challenges in marine and coastal environments: from local to global governance," *Restoration Ecology*, vol. 25, no. 1, pp. 123–128, 2017.

[4] S. L. Wong, N. Ngadi, T. A. T. Abdullah, and I. M. Inuwa, "Current state and future prospects of plastic waste as source of fuel: a review," *Renewable and Sustainable Energy Reviews*, vol. 50, pp. 1167–1180, 2015.

[5] N. Chaukura, W. Gwenzi, T. Bunhu, D. T. Ruziwa, and I. Pumure, "Potential uses and value-added products derived from waste polystyrene in developing countries: a review," *Resources, Conservation and Recycling*, vol. 107, pp. 157–165, 2016.

[6] T. P. Haider, C. Völker, J. Kramm, K. Landfester, and F. R. Wurm, "Kunststoffe der zukunft? Der einfluss von bioabbaubaren polymeren auf umwelt und gesellschaft," *Angewandte Chemie*, vol. 131, no. 1, pp. 50–63, 2019.

[7] S. Huysman, J. De Schaepmeester, K. Ragaert, J. Dewulf, and S. De Meester, "Performance indicators for a circular economy: a case study on post-industrial plastic waste," *Resources, Conservation and Recycling*, vol. 120, pp. 46–54, 2017.

[8] T. Leejarkpai, T. Mungcharoen, and U. Suwanmanee, "Comparative assessment of global warming impact and eco-efficiency of PS (polystyrene), PET (polyethylene terephthalate) and PLA (polylactic acid) boxes," *Journal of Cleaner Production*, vol. 125, pp. 95–107, 2016.

[9] E. J. North and R. U. Halden, "Plastics and environmental health: the road ahead," *Reviews on Environmental Health*, vol. 28, no. 1, pp. 1–8, 2013.

[10] J. E. Weinstein, B. K. Crocker, and A. D. Gray, "From macroplastic to microplastic: degradation of high-density polyethylene, polypropylene, and polystyrene in a salt marsh habitat," *Environmental Toxicology and Chemistry*, vol. 35, no. 7, pp. 1632–1640, 2016.

[11] B. M. Dominguez-Martinez, H. E. Martínez-Flores, J. D. J. Berrios, C. G. Otoni, D. F. Wood, and G. Velazquez, "Physical characterization of biodegradable films based on chitosan,

polyvinyl alcohol and Opuntia mucilage," *Journal of Polymers and the Environment*, vol. 25, no. 3, pp. 683–691, 2017.

[12] M. C. Lin, C. W. Lou, J. Y. Lin, T. A. Lin, Y. S. Chen, and J. H. Lin, "Biodegradable polyvinyl alcohol vascular stents: structural model and mechanical and biological property evaluation," *Materials Science and Engineering: C*, vol. 91, pp. 404–413, 2018.

[13] J. Jalvandi, M. White, Y. Gao, Y. B. Truong, R. Padhye, and I. L. Kyratzis, "Polyvinyl alcohol composite nanofibres containing conjugated levofloxacin- chitosan for controlled drug release," *Materials Science and Engineering: C*, vol. 73, pp. 440–446, 2017.

[14] K. P. Y. Shak, Y. L. Pang, and S. K. Mah, "Nanocellulose: recent advances and its prospects in environmental remediation," *Beilstein Journal of Nanotechnology*, vol. 9, no. 1, pp. 2479–2498, 2018.

[15] Y. H. Feng, T. Y. Cheng, W. G. Yang et al., "Characteristics and environmentally friendly extraction of cellulose nanofibrils from sugarcane bagasse," *Industrial Crops and Products*, vol. 111, pp. 285–291, 2018.

[16] A. L. M. P. Leite, C. D. Zanon, and F. C. Menegalli, "Isolation and characterization of cellulose nanofibers from cassava root bagasse and peelings," *Carbohydrate Polymers*, vol. 157, pp. 962–970, 2017.

[17] S. Nie, K. Zhang, X. Lin et al., "Enzymatic pretreatment for the improvement of dispersion and film properties of cellulose nanofibrils," *Carbohydrate Polymers*, vol. 181, pp. 1136–1142, 2018.

[18] D. Yue and X. Qian, "Isolation and rheological characterization of cellulose nanofibrils (CNFs) from coir fibers in comparison to wood and cotton," *Polymers (Basel)*, vol. 10, no. 3, p. 320, 2018.

[19] C. C. S. Coelho, M. Michelin, M. A. Cerqueira et al., "Cellulose nanocrystals from grape pomace: production, properties and cytotoxicity assessment," *Carbohydrate Polymers*, vol. 192, pp. 327–336, 2018.

[20] S. Collazo-Bigliardi, R. Ortega-Toro, and A. Chiralt Boix, "Isolation and characterisation of microcrystalline cellulose and cellulose nanocrystals from coffee husk and comparative study with rice husk," *Carbohydrate Polymers*, vol. 191, pp. 205–215, 2018.

[21] J. Lamaming, R. Hashim, C. P. Leh, and O. Sulaiman, "Properties of cellulose nanocrystals from oil palm trunk isolated by total chlorine free method," *Carbohydrate Polymers*, vol. 156, pp. 409–416, 2017.

[22] R. A. Ilyas, S. M. Sapuan, and M. R. Ishak, "Isolation and characterization of nanocrystalline cellulose from sugar palm fibres (Arenga pinnata)," *Carbohydrate Polymers*, vol. 181, pp. 1038–1051, 2018.

[23] S. Naduparambath, T. V. Jinitha, V. Shaniba, M. P. Sreejith, A. K. Balan, and E. Purushothaman, "Isolation and characterisation of cellulose nanocrystals from sago seed shells," *Carbohydrate Polymers*, vol. 180, pp. 13–20, 2018.

[24] J. P. De Mesquita, C. L. Donnici, I. F. Teixeira, and F. V. Pereira, "Bio-based nanocomposites obtained through covalent linkage between chitosan and cellulose nanocrystals," *Carbohydrate Polymers*, vol. 90, no. 1, pp. 210–217, 2012.

[25] A. Dufresne, "Processing of polymer nanocomposites reinforced with polysaccharide nanocrystals," *Molecules*, vol. 15, no. 6, pp. 4111–4128, 2010.

[26] E. Fortunati, I. Armentano, Q. Zhou et al., "Multifunctional bionanocomposite films of poly(lactic acid), cellulose nanocrystals and silver nanoparticles," *Carbohydrate Polymers*, vol. 87, no. 2, pp. 1596–1605, 2012.

[27] K. M. Chin, S. Sung Ting, H. L. Ong, and M. Omar, "Surface functionalized nanocellulose as a veritable inclusionary material in contemporary bioinspired applications: a review," *Journal of Applied Polymer Science*, vol. 135, no. 13, p. 46065, 2018.

[28] J. A. Sirviö, S. Honkaniemi, M. Visanko, and H. Liimatainen, "Composite films of poly(vinyl alcohol) and bifunctional cross-linking cellulose nanocrystals," *ACS Applied Materials & Interfaces*, vol. 7, no. 35, pp. 19691–19699, 2015.

[29] T. Song, S. Tanpichai, and K. Oksman, "Cross-linked polyvinyl alcohol (PVA) foams reinforced with cellulose nanocrystals (CNCs)," *Cellulose*, vol. 23, no. 3, pp. 1925–1938, 2016.

[30] A. K. Sonker, N. Tiwari, R. K. Nagarale, and V. Verma, "Synergistic effect of cellulose nanowhiskers reinforcement and dicarboxylic acids crosslinking towards polyvinyl alcohol properties," *J. Polym. Sci. Part A Polym. Chem.*, vol. 54, no. 16, pp. 2515–2525, 2016.

[31] S. A. Stone, P. Gosavi, T. J. Athauda, and R. R. Ozer, "In situ citric acid crosslinking of alginate/polyvinyl alcohol electrospun nanofibers," *Materials Letters*, vol. 112, pp. 32–35, 2013.

[32] S. Wang, J. Ren, W. Li, R. Sun, and S. Liu, "Properties of polyvinyl alcohol/xylan composite films with citric acid," *Carbohydrate Polymers*, vol. 103, no. 1, pp. 94–99, 2014.

[33] Y. Dou, B. Zhang, M. He, G. Yin, Y. Cui, and I. N. Savina, "Keratin/polyvinyl alcohol blend films cross-linked by dialdehyde starch and their potential application for drug release," *Polymers (Basel)*, vol. 7, no. 3, pp. 580–591, 2015.

[34] J. Li, Y. Li, Y. Song, S. Niu, and N. Li, "Ultrasonic-assisted synthesis of polyvinyl alcohol/phytic acid polymer film and its thermal stability, mechanical properties and surface resistivity," *Ultrasonics Sonochemistry*, vol. 39, no. May, pp. 853–862, 2017.

[35] M. Lim, H. Kwon, D. Kim, J. Seo, H. Han, and S. B. Khan, "Highly-enhanced water resistant and oxygen barrier properties of cross-linked poly(vinyl alcohol) hybrid films for packaging applications," *Progress in Organic Coatings*, vol. 85, pp. 68–75, 2015.

[36] P. Maji, A. Gandhi, S. Jana, and N. Maji, "Preparation and characterization of maleic anhydride cross-linked chitosan-polyvinyl alcohol hydrogel matrix transdermal patch," *Journal of PharmaSciTech*, vol. 2, no. 2, pp. 62–67, 2013.

[37] A. K. Sonker, H. D. Wagner, R. Bajpai, R. Tenne, and X. M. Sui, "Effects of tungsten disulphide nanotubes and glutaric acid on the thermal and mechanical properties of polyvinyl alcohol," *Composites Science and Technology*, vol. 127, pp. 47–53, 2016.

[38] Z. Wu, J. Wu, T. Peng et al., "Preparation and application of starch/polyvinyl alcohol/citric acid ternary blend antimicrobial functional food packaging films," *Polymers (Basel).*, vol. 9, no. 12, pp. 102–119, 2017.

[39] Y. An, T. Koyama, K. Hanabusa et al., "Preparation and properties of highly phosphorylated poly(vinyl alcohol) hydrogels chemically crosslinked by glutaraldehyde," *Polymer (Guildf)*, vol. 36, no. 11, pp. 2297–2301, 1995.

[40] X. Qin, G. Dou, G. Jiang, and S. Zhang, "Characterization of poly (vinyl alcohol) nanofiber mats cross-linked with glutaraldehyde," *Journal of Industrial Textiles*, vol. 43, no. 1, pp. 34–44, 2013.

[41] R. Rudra, V. Kumar, and P. P. Kundu, "Acid catalysed crosslinking of poly vinyl alcohol (PVA) by glutaraldehyde: effect of crosslink density on the characteristics of PVA membranes used in single chambered microbial fuel cells," *RSC Advances*, vol. 5, no. 101, pp. 83436–83447, 2015.

[42] K. Das, D. Ray, N. R. Bandyopadhyay et al., "Preparation and characterization of cross-linked starch/poly(vinylalcohol) green films with low moisture absorption," *Industrial and Engineering Chemistry Research*, vol. 49, no. 5, pp. 1520–5045, 2010.

[43] B. Sreedhar, D. K. Chattopadhyay, M. S. H. Karunakar, and A. R. K. Sastry, "Thermal and surface characterization of plasticized starch polyvinyl alcohol blends crosslinked with epichlorohydrin," *Journal of Applied Polymer Science*, vol. 101, no. 1, pp. 25–34, 2006.

[44] A. N. Frone, C. A. Nicolae, R. A. Gabor, and D. M. Panaitescu, "Thermal properties of water-resistant starch - polyvinyl alcohol films modified with cellulose nanofibers," *Polymer Degradation and Stability*, vol. 121, pp. 385–397, 2015.

[45] S. Liu, L. Wang, B. Zhang, B. Liu, J. Wang, and Y. Song, "Novel sulfonated polyimide/polyvinyl alcohol blend membranes for vanadium redox flow battery applications," *Journal of Materials Chemistry A*, vol. 3, no. 5, pp. 2072–2081, 2015.

[46] L. Chen, S. H. Imam, S. H. Gordon, and R. V. Greene, "Starch-polyvinyl alcohol crosslinked film— performance and biodegradation," *Journal of Environmental Polymer Degradation*, vol. 5, no. 2, pp. 111–117, 1997.

[47] M. Chaouat, C. le Visage, W. E. Baille et al., "A novel cross-linked poly(vinyl alcohol) (PVA) for vascular grafts," *Advanced Functional Materials*, vol. 18, no. 19, pp. 2855–2861, 2008.

[48] A. D. A. Morandim-Giannetti, R. C. Silva, O. Magalhães, P. Schor, and P. A. Bersanetti, "Conditions for obtaining polyvinyl alcohol/trisodium trimetaphosphate hydrogels as vitreous humor substitute," *Journal of Biomedical Materials Research Part B: Applied Biomaterials*, vol. 104, no. 7, pp. 1386–1395, 2016.

[49] C. H. Chan, C. H. Chia, S. Zakaria, I. Ahmad, and A. Dufresne, "Production and characterisation of cellulose and Nano-Crystalline cellulose from kenaf core wood," *BioResources*, vol. 8, no. 1, pp. 785–794, 2012.

[50] N. Amiralian, P. K. Annamalai, C. J. Garvey, E. Jiang, P. Memmott, and D. J. Martin, "High aspect ratio nanocellulose from an extremophile spinifex grass by controlled acid hydrolysis," *Cellulose*, vol. 24, no. 9, pp. 3753–3766, 2017.

[51] D. Liu, Y. Dong, D. Bhattacharyya, and G. Sui, "Novel sandwiched structures in starch/cellulose nanowhiskers (CNWs) composite films," *Composites Communications*, vol. 4, pp. 5–9, 2017.

[52] S. Mathew, J. Mathew, and E. K. Radhakrishnan, "Polyvinyl alcohol/silver nanocomposite films fabricated under the influence of solar radiation as effective antimicrobial food packaging material," *Journal of Polymer Research*, vol. 26, no. 9, pp. 1–10, 2019.

[53] K. M. Chin, S. T. Sam, H. L. Ong, Y. S. Wong, and W. K. Tan, "Biodegradation improvement of bioinspired crosslinked and noncrosslinked polyvinyl alcohol nanocomposites with cellulose nanocrystals extracted from rice straw through natural soil burial exposure," *Polymer Composites*, pp. 1–11, 2022.

[54] W. P. Flauzino Neto, H. A. Silvério, N. O. Dantas, and D. Pasquini, "Extraction and characterization of cellulose nanocrystals from agro-industrial residue - soy hulls," *Industrial Crops and Products*, vol. 42, pp. 480–488, 2013.

[55] A. Kumar, Y. Singh Negi, V. Choudhary, and N. K. Bhardwaj, "Characterization of cellulose nanocrystals produced by acid-hydrolysis from sugarcane bagasse as agro-waste "Characterization of cellulose nanocrystals produced by acid-hydrolysis from sugarcane bagasse as agro-waste," *Journal of Materials Physics and Chemistry*, vol. 2, no. 1, pp. 1–8, 2014.

[56] M. R. K. Sofla, R. J. Brown, T. Tsuzuki, and T. J. Rainey, "A comparison of cellulose nanocrystals and cellulose nanofibres extracted from bagasse using acid and ball milling methods," *Advances in Natural Sciences: Nanoscience and Nanotechnology*, vol. 7, no. 3, p. 035004, 2016.

[57] A. Saxena, M. Foston, M. Kassaee, T. J. Elder, and A. J. Ragauskas, "Biopolymer nanocomposite films reinforced with nanocellulose whiskers," *Journal of Nanoscience and Nanotechnology*, vol. 12, no. 1, pp. 218–226, 2012.

[58] A. H. A. Hoseini, M. Arjmand, U. Sundararaj, and M. Trifkovic, "Significance of interfacial interaction and agglomerates on electrical properties of polymer-carbon nanotube nanocomposites," *Materials and Design*, vol. 125, no. - April, pp. 126–134, 2017.

[59] D. Nataraj, S. Sakkara, M. Meghwal, and N. Reddy, "Cross-linked chitosan films with controllable properties for commercial applications," *International Journal of Biological Macromolecules*, vol. 120, pp. 1256–1264, 2018.

[60] H. Wu, Y. Lei, J. Lu et al., "Effect of citric acid induced crosslinking on the structure and properties of potato starch/chitosan composite films," *Food Hydrocolloids*, vol. 97, p. 105208, 2019.

[61] N. Jain, A. Verma, and V. K. Singh, "Dynamic mechanical analysis and creep-recovery behaviour of polyvinyl alcohol based cross-linked biocomposite reinforced with basalt fiber," *Materials Research Express*, vol. 6, no. 10, p. 105373, 2019.

[62] Y. Chen, J. Zhu, H. Y. Yu, and Y. Li, "Fabricating robust soft-hard network of self-healable polyvinyl alcohol composite films with functionalized cellulose nanocrystals," *Composites Science and Technology*, vol. 194, p. 108165, 2020.

[63] P. Lu and Y. Lo Hsieh, "Preparation and characterization of cellulose nanocrystals from rice straw," *Carbohydrate Polymers*, vol. 87, no. 1, pp. 564–573, 2012.

[64] H. Yu, H. Zhang, M. Song, Y. Zhou, J. Yao, and Q. Ni, "From cellulose nanospheres, nanorods to nanofibers: various aspect ratio induced nucleation/reinforcing effects on polylactic acid for robust-barrier food packaging," *ACS Applied Materials & Interfaces*, vol. 9, no. 50, pp. 43920–43938, 2017.

[65] J. Rhim, J. P. Reddy, and X. Luo, "Isolation of cellulose nanocrystals from onion skin and their utilization for the preparation of agar-based bio-nanocomposites films and their utilization for the preparation of agar-based bio-nanocomposites films," *Cellulose*, vol. 22, no. 1, pp. 407–420, 2015.

[66] Q. Wu, Y. Meng, K. Concha et al., "Influence of temperature and humidity on nano-mechanical properties of cellulose nanocrystal films made from switchgrass and cotton," *Industrial Crops and Products*, vol. 48, pp. 28–35, 2013.

[67] C. Liu, B. Li, H. du et al., "Properties of nanocellulose isolated from corncob residue using sulfuric acid, formic acid, oxidative and mechanical methods," *Carbohydrate Polymers*, vol. 151, pp. 716–724, 2016.

[68] P. Phanthong, P. Reubroycharoen, X. Hao, G. Xu, A. Abudula, and G. Guan, "Nanocellulose: extraction and application," *Carbon Resources Conversion*, vol. 1, no. 1, pp. 32–43, 2018.

[69] K. Choo, Y. C. Ching, C. H. Chuah, S. Julai, and N. S. Liou, "Preparation and characterization of polyvinyl alcohol-chitosan composite films reinforced with cellulose nanofiber," *Materials (Basel)*, vol. 9, no. 8, p. 644, 2016.

[70] J. Jose and M. A. Al-Harthi, "Citric acid crosslinking of poly(-vinyl alcohol)/starch/graphene nanocomposites for superior properties," *Iranian Polymer Journal*, vol. 26, no. 8, pp. 579–587, 2017.

[71] Z. Cui, Z. Zheng, L. Lin et al., "Electrospinning and crosslinking of polyvinyl alcohol/chitosan composite nanofiber for transdermal drug delivery," *Advances in Polymer Technology*, vol. 37, no. 6, p. 1928, 2018.

[72] E. Lizundia, E. Fortunati, F. Dominici et al., "PLLA-grafted cellulose nanocrystals: role of the CNC content and grafting on the PLA bionanocomposite film properties," *Carbohydrate Polymers*, vol. 142, pp. 105–113, 2016.

[73] T. Ben Shalom, Y. Nevo, D. Leibler et al., "Cellulose nanocrystals (CNCs) induced crystallization of polyvinyl alcohol (PVA) super performing nanocomposite films," *Macromolecular Bioscience*, vol. 19, no. 3, p. 1800347, 2019.

[74] P. A. Sreekumar, M. A. Al-Harthi, and S. K. De, "Reinforcement of starch/polyvinyl alcohol blend using nano-titanium dioxide," *Journal of Composite Materials*, vol. 46, no. 25, pp. 3181–3187, 2012.

[75] M. D. Stelescu, A. Airinei, E. Manaila et al., "Effects of electron beam irradiation on the mechanical, thermal, and surface properties of some EPDM/butyl rubber composites," *Polymers (Basel)*, vol. 10, no. 11, pp. 1206–1221, 2018.

[76] A. K. Sonker, K. Rathore, R. K. Nagarale, and V. Verma, "Crosslinking of polyvinyl alcohol (PVA) and effect of crosslinker shape (aliphatic and aromatic) thereof," *Journal of Polymers and the Environment*, vol. 26, no. 5, pp. 1782–1794, 2018.

[77] M. Song, H. Yu, J. Gu, S. Ye, and Y. Zhou, "Chemical crosslinked polyvinyl alcohol/cellulose nanocrystal composite films with high structural stability by spraying Fenton reagent as initiator," *International Journal of Biological Macromolecules*, vol. 113, no. 2017, pp. 171–178, 2018.

[78] M. P. Weir, D. W. Johnson, S. C. Boothroyd et al., "Distortion of chain conformation and reduced entanglement in polymer-graphene oxide nanocomposites," *ACS Macro Letters*, vol. 5, no. 4, pp. 430–434, 2016.

[79] R. Maria and H. Poetes, *Dynamic and Static Conformations at the Water-Solid Interface*, University of Cambridge, 2009.

[80] C. Rieu, L. Bertinetti, R. Schuetz et al., "The role of water on the structure and mechanical properties of a thermoplastic natural block co-polymer from squid sucker ring teeth," *Bioinspiration & Biomimetics*, vol. 11, no. 5, pp. 1–10, 2016.

[81] S. S. Nair, J. Zhu, Y. Deng, and A. J. Ragauskas, "High performance green barriers based on nanocellulose," *Sustainable Chemical Processes*, vol. 2, no. 1, pp. 1–7, 2014.

[82] J. Wang, D. J. Gardner, N. M. Stark, D. W. Bousfield, M. Tajvidi, and Z. Cai, "Moisture and oxygen barrier properties of cellulose nanomaterial-based films," *ACS Sustainable Chemistry & Engineering*, vol. 6, no. 1, pp. 49–70, 2018.

[83] W. Ma, P. Zhang, B. Zhao et al., "Swelling resistance and mechanical performance of physical crosslink-based poly(vinyl alcohol) hydrogel film with various molecular weight," *Journal of Polymer Science Part B: Polymer Physics*, vol. 57, no. 24, pp. 1673–1683, 2019.

[84] P. A. Bersanetti, V. H. Escobar, R. F. Nogueira, F. dos Santos Ortega, P. Schor, and A. de Araújo Morandim-Giannetti, "Enzymatically obtaining hydrogels of PVA crosslinked with ferulic acid in the presence of laccase for biomedical applications," *European Polymer Journal*, vol. 112, pp. 610–618, 2019.

[85] B. Singh and A. Kumar, "Graft and crosslinked polymerization of polysaccharide gum to form hydrogel wound dressings for drug delivery applications," *Carbohydrate Research*, vol. 489, p. 107949, 2020.